Macromolecular Materials and Engineering
Open Access
www.mame-journal.de

Thermo-Compressed Films of Poly(butylene succinate) Reinforced with Cellulose Fibers Obtained from Rice Straw by Green Extraction Methods

Carmen Olivas-Alonso, Pedro A. V. Freitas, Sergio Torres-Giner, and Amparo Chiralt*

In this study, two green extraction methods are explored to valorize rice straw into cellulose fibers (CFs), namely subcritical water extraction (SWE) and combined ultrasound-heating treatment (USHT). The resultant fibers are, thereafter, successfully pretreated with (3-glycidyloxypropyl) trimethoxysilane (GPS) and incorporated at 3% wt into poly(butylene succinate) (PBS) by melt-mixing. The green composites are shaped into films by thermo-compression and characterized in terms of their performance for food packaging applications. The chemical analysis of the fibers reveals that SWE is more effective to selectively remove hemicelluloses than USHT, whereas silanization promotes the removal of lignin in both fiber types. Fiber incorporation, more notably in the case of the silanized fibers, restricts the movement of the PBS chains, indicating good interaction with the biopolyester matrix. In particular, CFs act as antinucleating agents in PBS, delaying both glass transition and crystallization from the melt phenomena and hindering crystal formation. Furthermore, the fibers mechanically reinforce and improve the oxygen barrier of the PBS films. The highest barrier enhancement is obtained for the thermo-compressed composite film with silanized fibers obtained by SWE, yielding a decrease of nearly 20% in the permeability to oxygen versus the unfilled PBS film.

1. Introduction

The increase in environmental awareness within modern society has led to the development of renewable materials and biodegradable products that follow a productive circular model.[1] Such growing environmental concerns are particularly pronounced in the case of food packaging since it represents a constant source of high amounts of plastic waste. One of the most reliable and sustainable alternatives in food packaging is the development of bio-based and biodegradable polymers. The so-called biopolymers are macromolecules that are obtained from biomass and can disintegrate in industrial compost or natural media, which include proteins, polysaccharides and, most relevantly, biopolyesters.[1] In particular, polyesters derived from renewable succinic acid, such as poly(butylene succinate) (PBS) and its copolymers, are considered among the most promising materials to replace polyolefins since these can be processed with conventional plastic equipment and combine good mechanical, thermal, and barrier properties.[2] PBS is a biodegradable semicrystalline aliphatic polyester that is obtained via polycondensation reaction of succinic acid and 1,4-butanediol. Although it has been exclusively a petrochemical polymer, since recently succinic acid can also be produced from sugar-rich compounds by bacterial fermentation routes.[3] This results in partially bio-based PBS, showing the same performance that its petrochemical counterpart.[4]

However, the use of renewable succinic acid derived polyesters for food packaging purposes is still limited due to their high cost and lower properties compared to petrochemical polymers.[5] Different alternatives and approaches have been investigated to improve the performance of PBS and other biopolymers, for example, the use of fillers to produce green composites.[6] Beside reducing expenses, filler incorporation can also enable the improvement of the thermal and mechanical properties of the biopolymer matrices. Furthermore, from an environmental viewpoint, agricultural and food residues are perfect candidates. Among them, rice straw is very promising since it is one of the most abundant lignocellulosic waste materials and presents a high content of cellulose (36.7%).[7] Moreover, rice straw shows excellent biodegradability and good thermal stability.[8] Nevertheless, extracting the cellulose fibers (CFs) from the agri-food wastes requires the purification of the lignocellulosic fractions from the plant matrix, which can be challenging due to the recalcitrant structure of the hemicellulose-cellulose-lignin complexes and silica.[7] Chemical methods, such as the traditional alkaline treatment, involve the use of a significant quantity of chemicals so that the use of water-based and physical methods offers a more sustainable alternative. For instance, an eco-friendly and cost-effective option is the use of subcritical water extraction (SWE) to eliminate a great part of noncellulosic

C. Olivas-Alonso, P. A. V. Freitas, S. Torres-Giner, A. Chiralt
University Institute of Food Engineering—FoodUPV
Universitat Politècnica de València (UPV)
Camino de Vera s/n, Valencia 46022, Spain
E-mail: storresginer@upv.es

DOI: 10.1002/mame.202400094

components.[9] Operating under subcritical water conditions (at high temperature and pressure, below the critical point) the properties of water change, exhibiting solvent properties similar to some organic solvents, such as methanol or ethanol.[10] This enhances the limited water affinity with low polar substances present in the natural lignocellulosic residues. In particular, the decrease in the dielectric constant, surface tension, density, and viscosity of water facilitate its diffusion and penetration into the plant matrix.[11] Furthermore, a new method for producing CFs with a higher yield than the conventional alkaline process is the combined ultrasound-heating treatment (USHT).[7] The application of ultrasound, prior to the heating treatment, generates acoustic cavitation, disrupting the structure of the plant cells and exposing inner tissues.[12] This results in a greater exposed surface with enhanced accessibility to the extracting solvent, weakening interactions between the noncellulosic components in the plant matrix. This contributes to improve the extraction efficiency in the subsequent heat-water extraction process.

In many studies, CFs have been incorporated into different biopolymers.[13] In most cases, development of green composites of polylactide (PLA) with different cellulosic structures have been analyzed.[14] Specifically, PBS has been reinforced with pretreated cotton stalk fibers, observing that these fillers acted as nucleation agents and physical hindrances to impede the movement of chain segments during nonisothermal crystallization.[15] Rice straw fibers, chemically treated to purify the cellulose and isolate smooth cellulose microfibrils, have been incorporated into poly(vinyl alcohol) (PVA) to enhance its water adsorption properties.[16] Nevertheless, the existing literature highlights the limited interfacial interaction between the hydrophobic polymers and hydrophilic fibers,[17] which consequently impacts negatively on the characteristics of the resulting green composites.[18] In particular, the presence of a large number of hydroxyl (—OH) groups on the cellulose surface results in a polar fiber surface with relatively low compatibility with the biopolymer matrices and a pronounced tendency for self-agglomeration.[19] Furthermore, as other lignocellulosic fibers, rice straw derived CFs are prone to moisture adsorption due to the abundance of free —OH groups on their surface. These inherent characteristics habitually results in a nonuniform dispersion and distribution of CFs during the melt-transformation processes, leading to a significant loss of performance in the green composites.[20,21]

In this context, different strategies have been carried out to reduce CF moisture adsorption capacity as well as to enhance the filler-matrix interaction in green composites to facilitate load transfer. These mainly include both chemical pretreatments of the fibers and the use of compatibilizers or coupling agents during the preparation of the composite.[22] For instance, silanization can modify the surface of cellulose, being yet a sustainable, scalable, and cost-effectiveness process with low energy requirements and benign solvent conditions.[23] The presence of multiple epoxy groups, which also appears in epoxidized compatibilizers, provides the silane pretreated fibers with a high reactivity, eliminating the requirement of potentially harmful solvents for dissolution.[24] In this sense, Liu et al.[25] conducted silanization on alkali-treated jute fibers for manufacturing PBS composites, resulting in composites with enhanced biodegradability compared with those without surface modification. The silanization process also removed a certain amount of lignin, hemicellulose, and pectin that covered the external surface of the fiber, improving the fibers-to-PBS adhesion and enhancing mechanical interlocking. In another study, Valadez-Gonzalez et al.[26] investigated the modification of henequen lignocellulosic fibers using vinyltris(2-methoxyethoxy) silane. The untreated henequen fibers displayed a characteristic load-displacement curve, indicating a suboptimal interphase compatibility between the hydrophilic fiber and the hydrophobic matrix. Silane-treated fibers exhibited a weakly bonded interphase, while the single fiber fragmentation test revealed elevated interfacial shear strength values that enhanced the interfacial load transfer efficiency. Zhao et al.[27] studied the effect of aminosilanes on the interaction mechanism between PBS and rice straw fibers with diameters in the 100–1000 μm range. Authors found that the tensile strength of the fiber reinforced PBS composites increased sharply with low amounts of silane. However, the tensile strength of the composites began to decrease upon adding more silane amounts until reaching a plateau, point at which the minimum interfacial saturation value for a coupling agent was achieved. Calabia et al.[28] reinforced PBS with cotton fibers treated with three different silanes, including trimethoxy silane. The tensile strength of the green composites was studied with fiber contents varying from 0 to 3% wt. Composites treated with trimethoxy silane achieved the highest tensile strength with 3% wt of fibers.

The aim of this study was to explore the use of CFs obtained by green extraction methods (without alkaline treatment) to reinforce PBS films. To this end, the fibers were first obtained by applying two aqueous extraction methods, one based on subcritical water at 180 °C, named SWE, and other that combined ultrasound pretreatment and heating with reflux water, called USHT. Thereafter, the cellulose fractions were submitted to a bleaching treatment with sodium chlorite to purify the fibers, herein respectively referred as SWE-CF and USHT-CF. After this, both types of fibers were subjected to silanization, resulting in the so-called SWE-SCF and USHT-SCF, respectively, to improve their compatibility with PBS. Then, the silanized and nonsilanized CFs were finally incorporated into PBS at 3% wt by melt-mixing and the resultant dough was subsequently shaped into films by thermo-compression. The effect of the incorporation of each type of CF on the thermal, mechanical, and barrier properties of the biopolyester was analyzed and related to the chemical composition of the fibers and the resultant microstructure of the green composites.

2. Experimental Section

2.1. Materials

Rice straw (*Oryza sativa* L.), J. Sendra variety, was collected in the L'Albufera rice paddy (Valencia, Spain). The as-received agricultural waste was dried for 16 h at 50 ± 2 °C under vacuum (VACIOTEM-T 4001489, J.P. Selecta, S.A., Barcelona, Spain). Afterward, the plant material was ground for 3 cycles of 90 s at 12 000 rpm (Thermomix TM6, España M.S.L., S.C., Madrid, Spain), sieved to collect particles under 0.5 mm, and then stored until further use in airtight glass bottles at 20 ± 2 °C to prevent sample hydration.

The PBS biopolyester was supplied, in the form of pellets, by Mitsubishi Chemical Corporation (Tokyo, Japan) as BioPBS

FZ71PM. This polyester grade is partially bio-based due to it is derived from renewable succinic acid. It is designed to be intended to come in contact with food since it complies to EU No.10/2011 and is also biodegradable under industrial composting conditions with the "OK Compost" certification (EN 13432).

A glycidyl silane, namely (3-glycidyloxypropyl) trimethoxysilane, hereinafter referred to as GPS, was purchased from Sigma-Aldrich S.A. (Madrid, Spain) with CAS number 2530-83-8, molecular weight (M_W) of 236.34 g mol^{-1}, and density of 1.07 g cm^{-3}.

Glacial acetic acid, ethanol, acetone, magnesium nitrate ($Mg(NO_3)_2$), and di-phosphorus pentoxide (P_2O_5) were all supplied by Panreac Quimica S.L.U. (Castellar del Vallés, Spain). Sodium acetate and sodium chlorite were both purchased from Honeywell International Inc. (Offenbach am Main, Germany).

2.2. Extraction and Silanization of Cellulose Fibers

Prior to the bleaching step, two different water-based extraction treatments, that is, SWE and USHT, were performed on rice straw according to the previous findings.[7,9] These methods gave rise to CFs extracted by SWE and USHT that were afterward used without pretreatment (SWE-CF and USHT-CF) or silanized (SWE-SCF and USHT-SCF).

2.2.1. Subcritical Water Extraction

SWE was carried out using a ratio of rice straw and distilled water of 1:10 wt/v. The SWE process was performed in a pressure reactor (Model 1-T-A-P-CE, 5 L capacity, Amar Equipment PVT. LTD, Mumbai, India) at 180 °C (11 bars due to the water vapor pressure) and 150 rpm for 30 min. Afterward, the dispersion was cooled to 30 °C and filtered (Filterlab, Vidrafoc, Barcelona, Spain). The filtration residue was gently washed with distilled water to remove the retained soluble fractions. Then, this residue was vacuum dried (VACIOTEM-T 4001489, S.P. Selecta, S.A.) at 35 °C for 24 h to determine the step yield and milled (IKA, model M20, IKA Werke GmbH & Co. KG, Staufen, Germany), applying pulses of 2 s for 20 min.

2.2.2. Combined Ultrasound-Heating Treatment

A sequential method consisting of a combination of ultrasound and heating treatment, the so-called USHT, was applied. Briefly, a 5% wt/v aqueous dispersion of rice straw was first immersed in an ice bath, while ultrasonicated for 30 min, using a probe high-intensity ultrasonic homogenizer (Vibra Cell VCX750, 750 W power, Sonics & Material Inc., Newtown, CT, USA), operating at a frequency of 20 kHz, 40% sonication amplitude, in continuous mode. Afterward, the dispersion was heated at reflux conditions (100 °C) for 1 h, filtered, and washed with distilled water three times. Finally, the insoluble fraction was vacuum dried (VACIOTEM-T 4001489) at 35 °C for 48 h and milled (IKA M20), applying pulses of 2 s for 20 min.

2.2.3. Bleaching

The solid residues obtained from both extraction techniques were, thereafter, bleached following the previously optimized conditions.[7] To this end, the dry samples were first mixed at 5% wt with a bleaching solution prepared by mixing equal parts of distilled water, acetate buffer solution (2 N), and sodium chlorite 1.7% (wt/v). The suspension was then treated under reflux heating at 100 °C for 4 h. Thereafter, the solid fraction was filtered and washed with distilled water to remove the residual bleaching solution. The procedure was repeated four times. Then, the bleached samples obtained from each extraction method (named as SWE-CF and USHT-CF) were vacuum dried (VACIOTEM-T 4001489) at 35 °C for 48 h, milled (IKA M20) applying pulses of 1 s for 20 min, and finally stored in desiccators with P_2O_5 at 25 °C.

2.2.4. Silanization

Silanization was performed using GPS based on the procedure described by Cabrera et al.[24] First, an aqueous suspension with 1% wt of bleached CF was ultrasonicated in an ice bath for 20 min (Vibra Cell VCX750, 20 kHz, 40%, continuous mode). Afterward, 3% wt GPS with respect to the CF content was added to the dispersion. Thus, pH was adjusted to 3 by adding glacial acetic acid to hydrolyze the alkoxy groups of the silane to silanol groups.[27] At the next step, physisorption of silanol was promoted by stirring the dispersion for 4 h at 45 °C. After this, the dispersion was filtered and washed with an ethanol/water mixture 8:2 v/v and then with acetone to remove both acetic acid and weakly adsorbed silane molecules. Hereafter, condensation reaction of the cellulose hydroxyls and silanol was performed at 120 °C for 12 h in a vacuum oven (VACIOTEM-T 4001489). Last step involved a Soxhlet extraction in acetone for 12 h to eliminate any residue of nonbonded silane to the cellulosic fibers. Finally, the acetone solvent used during silanization was rotary evaporated and recovered.

2.3. Characterization of Cellulose Fibers

The resultant CFs were characterized in terms of their chemical composition, microstructure, and thermal stability. Prior to the different analysis, the samples were conditioned in desiccators with P_2O_5 at 25 ± 2 °C for, at least, 1 week to ensure dryness.

2.3.1. Chemical Analysis

Structural carbohydrate and lignin contents were analyzed in the fibers applying the NEREL method (NREL/TP-510-42618).[29] A two-step sulfuric acid hydrolysis was conducted on both the bleached and silanized fibers. The Klason lignin content, deduced from the acid-insoluble fraction, was assessed gravimetrically. Glucose, xylose, and arabinose was quantified in the acid-soluble fractions using high-performance liquid chromatography (HPLC) with a liquid chromatograph (Agilent Technologies, model 1120 Compact LC, Santa Clara, USA) equipped with a Rezex RCM-Monosaccharide Ca^{2+} column (150 mm × 7.8 mm) and an evaporative light scattering detector (ELSD Agilent Technologies 1200 Series, Waldbronn, Germany). The mobile phase was deionized water, in an isocratic mode, at a flow-rate of 0.4 mL min^{-1}. The detector was set at the conditions of 40 °C, 3.0 bar gas

pressure (N_2), and a gain of 3. The software used was ChemStation (version LTS 01.11, Agilent Technologies, Waldbronn, Germany) and data were analyzed with the Origin program (version OriginPro 2021, OriginLab Corporation, Northampton, MA, USA) by applying the Gaussian model for peak area determination. Hemicellulose content was calculated by the sum of xylose and arabinose contents, whereas cellulose content was derived from glucose concentration, as described by Sluiter et al.[29] These analyses were performed in duplicate for each sample.

2.3.2. Microscopy

The morphology of the CFs was evaluated using a field emission scanning electron microscope (FESEM) equipped with focused ion gun (AURIGA Compact, Zeiss, Oxford Instruments, UK). Images were taken 1.0 kV acceleration voltage with different magnifications. Fiber diameters were measured from the FESEM micrographs at different points with the ImageJ software (National Institute of Health, Bethesda, MD, USA), taking 75 measurements for each sample.[30]

2.3.3. Thermogravimetric Analysis

The bleached cellulose fibers before (SWE-CF and USHT-CF) and after silanization (SWE-SCF and USHT-SCF) were subjected to thermogravimetric analysis (TGA) in a thermal analyzer (TGA 1 Stare System analyzer, Mettler-Toledo GmbH, Greifensee, Switzerland). Samples of about 4–5 mg were weighed into alumina pans and heated from 25 to 700 °C. The following values were obtained from the TGA curves and their first derivative thermogravimetric analysis (DTGA) curves: the mass loss percentage attained at 140 °C corresponding to moisture (Δ_{m_1}), the onset degradation temperature (T_{onset}), the temperature at the maximum degradation rate (T_{peak}), the mass loss percentage attained at the second thermal event (Δ_{m_2}), the mass loss percentage attained at the third event (Δ_{m_3}), and the residual mass at 700 °C. Measurements were performed by triplicate for each sample.

2.4. Composite Films Preparation

2.4.1. Melt-Mixing

PBS and CFs were melt-mixed in an internal mixer (HAAKETM PolyLabTM QC, Thermo Fisher Scientific, Germany). A 3% wt loading of each fiber (SWE-CF, USHT-CF, SWE-SCF, and USHT-SCF) was selected on the basis of a previous study.[31] The mixing process was performed at 50 rpm for 5 min at 150 °C. The resultant doughs were milled with liquid nitrogen in a Thermomix TM6 (Vorwerk, Valencia, Spain) and dried at 0% HR in desiccators with P_2O_5 for 24 h.

2.4.2. Thermo-Compression

The resulting powders were, thereafter, shaped into films by thermo-compression in a hydraulic press (Model LP20, Labtech Engineering Co., Ltd., Thailand). This process consisted of a preheating at 150 °C for 4 min followed by compression at 150 °C and 100 bar for 5 min. Thermo-compressed PBS/CF films with thickness of about 240 µm were produced. A control film of PBS without CF was also prepared in the same conditions.

2.5. Composite Films Characterization

2.5.1. Thickness and Sample Conditioning

The film thicknesses were gauged using a digital micrometer (Palmer, COMECTA model, Barcelona, accuracy: 0.001 mm) at ten randomly chosen positions. The film samples were conditioned before the analyses at 0% or 53% relative humidity (HR) depending on the kind of analysis.

2.5.2. Microstructural Analyses

The dispersion of CFs in PBS was evaluated by optical microscopy. For this, the film samples were placed on a glass slide and observed at 40x magnification in an optical microscope (Optika Microscope B-350, OPTIKA Srl, Ponteranica, Italy) equipped with a camera (Optikam B2).

The internal structure of the film cross-sections was examined by FESEM. To this end, the samples were cryogenically fractured by immersing them in liquid nitrogen and then coated with platinum using an EM MED020 sputter coater (Leica BioSystems, Barcelona, Spain). Subsequently, images were captured in a FE-SEM equipped with focused ion gun (Auriga Compact) at 2.0 kV with different magnifications.

2.5.3. Thermal Analyses

The phase transitions of the PBS samples were investigated by differential scanning calorimetry (DSC) in a DSC823e Stare (Mettler-Toledo Inc., Switzerland) operating under a nitrogen atmosphere (10 mL min^{-1}). Samples (between 5 and 6 mg) were placed into aluminum pans and tightly sealed. Then, these were placed in the calorimeter and the following three-step program was applied: a first heating from −40 to 150 °C, followed by cooling to −40 °C, and then second heating to 150 °C. As the reference sample, an empty aluminum pan was used. Each sample was analyzed, in duplicate, using heating and cooling rates of 10 °C min^{-1}. Then, the degree of crystallinity (χ_c) was calculated by means of Equation (1)

$$\chi_c = \frac{\Delta H_m - \Delta H_{cc}}{\Delta H^\circ_m \cdot (1-\omega)} \cdot 100 \quad (1)$$

where ΔH_m and ΔH_{cc} correspond to the melting and cold crystallization enthalpies of PBS, respectively, both obtained from the second heating scan. ΔH°_m stands for the reported melting enthalpy of a fully crystalline PBS, which was 200 J g^{-1},[5,32] and ω represents the mass fraction of fiber in the composite.

Thermal stability was determined by TGA using a thermogravimetric analyzer (TGA 1 Stare System analyzer) from 25 to 700 °C. This analysis was performed in the same conditions described for the CF analysis.

2.5.4. Mechanical Test

The tensile properties of the films were assessed using a universal testing machine (TA.XTplus model, Stable Micro Systems, Haslemere, England) following the standard ASTM D882 procedure (ASTM, 2012). Film samples were trimmed to dimensions of 2.5 cm × 10 cm, placed in the film-extension grips (5 cm separation) of the testing machine, and elongated at a crosshead speed of 5 mm min^{-1} until fracture. At least seven samples per formulation were examined.

2.5.5. Thermomechanical Analysis

Dynamic mechanical thermal analysis (DMTA) of the film samples were carried out with a Discovery DHR-1 oscillatory rheometer (TA Instruments, New Castle, DE, USA) equipped with a clamp system for solid samples in torsion mode. Film samples sizing 5 mm × 15 mm were submitted to a heating program from −50 to 150 °C, with a heating rate of 2 °C min^{-1}, applying a maximum deformation (γ) of 0.1%, at a constant frequency of 1 Hz.

2.5.6. Permeability Tests

The water vapor permeability (WVP) of the films, expressed in kg m m^{-2} Pa s, was determined gravimetrically following ASTM E96/E96M (ASTM, 2005)[33] and the experimental procedure described by Hernández-García et al.[4] The samples were cut and placed in circular Payne cups (Ø = 3.5 cm) containing 5 mL of distilled water (100% RH). Then, the cups were put into desiccators at 25 °C and 53% RH (with $Mg(NO_3)_2$ over-saturated solution). The cups were weighed every 1.5 for 24 h and the water vapor transmission rate (WVTR) was determined from the slope of the weight loss versus time curve and corrected for permeant partial pressure to yield permeance. WVP was finally determined taken the film thickness into account. The measurements were taken in triplicate for each film.

Oxygen permeability (OP) was determined by following the ASTM standard method D3985 05.[4] For this, films of 50 cm^2 of each formulation were placed in an oxygen permeation analyser (Model 8101e, Systech Illinois, IL, USA) at 25 °C and 53% RH. OP was calculated by dividing the oxygen transmission rate (OTR) by the difference in oxygen partial pressure between the two sides of the film and multiplying by film thickness.

2.5.7. Water Contact-Angle Measurements

The wettability of the different films was characterized through the contact angle measurements, using an Easy drop standard goniometer model FM140 (Krüss Equipments, Hamburg, Germany). This is equipped with a video capture kit and analysis software (Drop Shape Analysis SW21; DSA1). The characterization was carried out at room temperature with distilled water droplets of ≈15 µL. The water contact angle was measured at 3 different points on the film surface and each measure was performed five times.

Table 1. Chemical composition in terms of cellulose, hemicellulose, and Klason lignin content of cellulose fibers obtained by subcritical water extraction and combined ultrasound-heating treatment before (SWE-CF, USHT-CF) and after silanization (SWE-SCF, USHT-SCF).

Sample	Cellulose [% wt]	Hemicellulose [% wt]	Klason Lignin [% wt]
SWE-CF	$68.7 \pm 1.4^{ab)}$	$3.4 \pm 0.4^{a)}$	$5.1 \pm 1.1^{a)}$
USHT-CF	$65.9 \pm 0.7^{a)}$	$15.6 \pm 0.4^{b)}$	$5.2 \pm 0.2^{a)}$
SWE-SCF	$72.9 \pm 2.3^{b)}$	$3.6 \pm 0.5^{a)}$	$0.6 \pm 0.2^{b)}$
USHT-SCF	$68.7 \pm 0.5^{ab)}$	$16.3 \pm 0.4^{b)}$	$1.7 \pm 0.5^{b)}$

[a,b)] Different superscripts in the same column indicate significant differences between samples ($p < 0.05$).

2.6. Statistical Analysis

Results were submitted to analysis of variance (ANOVA) using Statgraphics Centurion XVII-64 software (Manugistics Corp., Rockville, MD, USA). Significant differences were considered with a significance level greater than 95% ($p < 0.05$).

3. Results and Discussion

3.1. Properties of Cellulose Fibers

The composition analysis of the fibers is shown in **Table 1**. The values of cellulose content revealed that the SWE method was more effective to selectively remove hemicelluloses than the USHT method, while the lignin content was similar in both bleached fibers, as previously reported by other authors.[9,10] Likewise, the silanization process promoted the removal of lignin in both kinds of fibers, which can be related to the use of acetone during the final fiber washing due to the solvent chemical affinity with lignin components. These results are also consistent with the values reported by Liu et al.[25]

Figure 1 shows the FESEM micrographs of all bleached fibers. The fibers showed a smooth surface that can be ascribed to the effective removal of the noncellulose components (hemicelluloses, waxes, and lignin) during the extraction and bleaching treatments. Likewise, it can be observed the greater defibrillation of fiber bundles achieved in the SWE-CF samples (Figure 1a) in comparison with the USHT-CF samples (Figure 1b). This effect can be attributed to the higher elimination of hemicellulose during the extraction step, which could favor microfiber separation and was also reflected by a slight reduction in the fiber diameters of the bleached samples. After the silanization step, as seen in the bottom FESEM micrographs (Figure 1c,d), both types of fibers exhibited a higher degree of defibrillation. This effect was probably due to the additional lignin elimination during silanization, as also reported by Liu et al.[25] Both fibers also presented similar morphology and diameter, the USHT-SCF being slightly thicker than the SWE-SCF, as observed prior to silanization. The cellulose surfaces became rougher after silanization due to the formation of nanosized precipitates, which have been attributed to the silane clusters or agglomerates formed by the predominantly physisorbed glycidyl-silane molecules that form siloxane bonds (Si−O−Si) instead of bonding with the −OH groups on the cellulose surface. Clustering of silanes was reported in other

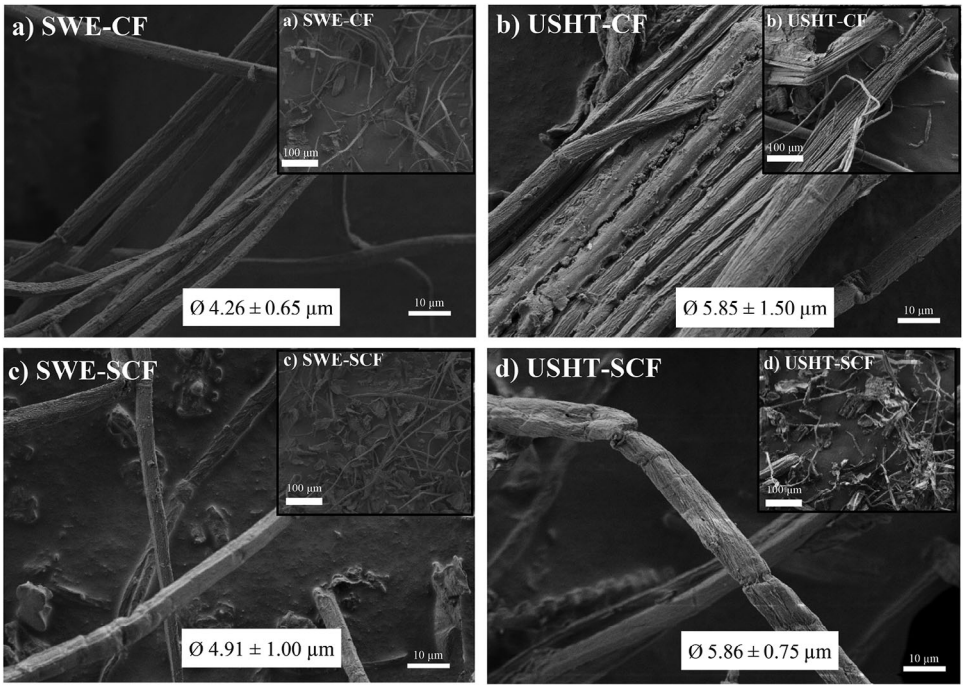

Figure 1. Field emission scanning electron microscope (FESEM) micrographs of cellulose fibers obtained by subcritical water extraction and combined ultrasound-heating treatment before and after silanization: a) SWE-CF. b) USHT-CF. c) SWE-SCF. d) USHT-SCF. Images taken at 1000x and inlets at 100x with scale markers of 10 and 100 µm, respectively.

studies dealing with the silanization of cellulose materials by dodecyltrichlorosilane and (3-glycidyloxypropyl)trimethoxysil.[4] Thus, small aggregates were highly dispersed across the fiber entire surface, creating a rougher surface. Nevertheless, a reduced self-adsorption of silane molecules could be deduced from the fiber roughness and, consequently, the presence of available glycidyl functional groups ready to react with the biopolymer matrix was expected.

Figure 2 shows the TGA curves (Figure 2a) and their corresponding DTGA curves (Figure 2b) obtained for the different the dried cellulosic samples, while **Table 2** summarizes the parameters determined for each thermal degradation event. The first and small loss weight in the temperature range from 30 to 140 °C corresponds to the mass loss percentage Δ_{m_1} that is associated to the loss of bonded water and other low-M_W volatiles.[34] Fiber samples obtained from the SWE process exhibited lower values than the ones from the USHT process, which reflects their higher hydrophobicity and this is related with the higher hemicellulose removal by this extraction method. Moreover, in these samples, silanization reduced significantly ($p < 0.05$) the water content, which suggests a larger replacement of the −OH in the cellulose chains by silanes. However, in the more hydrophilic USHT fibers, the silanization process did not provoke a reduction of the bonded water content in the fibers.

Hemicellulose, cellulose, and lignin fractions of lignocellulosic materials, such as rice straw, typically exhibit thermal degradation steps at temperature ranges of 150–350, 275–350, and 250–500 °C, respectively, although the lignin degradation could

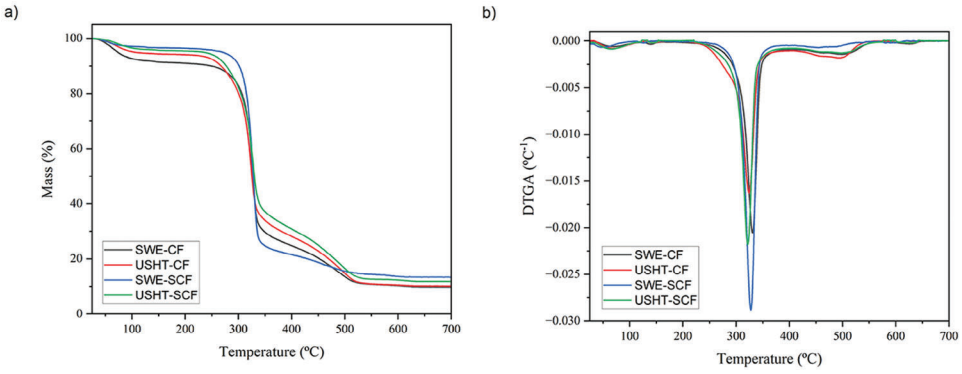

Figure 2. a) Thermogravimetric analysis (TGA) and b) first derivative thermogravimetric analysis (DTGA) curves of cellulose fibers obtained by subcritical water extraction and combined ultrasound-heating treatment before (SWE-CF, USHT-CF) and after silanization (SWE-SCF, USHT-SCF).

Table 2. Thermal decomposition events detected for cellulose fibers obtained by subcritical water extraction and combined ultrasound-heating treatment before (SWE-CF, USHT-CF) and after silanization (SWE-SCF, USHT-SCF).

Sample[a)]	Δ_{m_1} [%][a)]	[250–350] °C[a)]			[350–700] °C		
		T_{onset} [°C]	T_{peak} [°C]	Δ_{m_2} [%]	Δ_{m_3} [%]	T_{peak} [°C]	Residue [%]
SWE-CF	4.9 ± 1.2[b)]	308.4 ± 2.3[b)]	329.2 ± 3.4[d)]	57.9 ± 1.3[a)]	21.3 ± 1.6[a)]	497.5 ± 11.6[ab)]	11.0 ± 2.7[a)]
USHT-CF	3.0 ± 0.8[b)]	300.9 ± 2.9[a)]	321.8 ± 3.3[a)]	56.8 ± 1.4[a)]	25.7 ± 0.6[b)]	491.6 ± 10.9[a)]	12.1 ± 0.8[a)]
SWE-SCF	0.9 ± 0.5[a)]	307.1 ± 0.7[b)]	327.0 ± 1.5[bc)]	57.3 ± 1.3[a)]	18.8 ± 3.0[a)]	508.2 ± 2.5[b)]	21.5 ± 3.6[b)]
USHT-SCF	1.4 ± 1.1[a)]	302.0 ± 1.1[a)]	322.8 ± 1.0[ab)]	58.7 ± 2.6[b)]	22.1 ± 0.6[a)]	505.0 ± 2.9[ab)]	16.7 ± 1.3[c)]

[a–c)] Different superscripts in the same column indicate significant differences between samples ($p < 0.05$).

have a wider temperature range (160–900 °C) with a high residual mass.[9] For instance, Yang et al.[35] reported that cellulose pyrolysis occurred between 315 and 400 °C, with the maximum weight loss rate at 355 °C and a low residue. One can observe that all the fiber samples studied herein exhibited the typical thermodegradation profile of cellulose with small quantities of hemicellulose and lignin, as deduced from the composition analyses. The main thermal degradation event was seen in the 250–350 °C range, with a mass loss percentage Δ_{m_2} of nearly 60%, associated mainly to the cellulose degradation.[36] For the SWE-CF samples, the T_{peak} value was significantly ($p < 0.05$) higher, according to the greater cellulose content of this sample. In contrast, USHT samples exhibited a wider degradation peak due to overlapped degradation of residual hemicellulose. All samples showed a last thermal decomposition step (T_{peak} ranging from 490 to 508 °C), which was attributed to the thermal degradation of lignin and products deriving from the fragmentation of the organic structure, as reported by Theng et al.[37] No significant differences ($p > 0.05$) were found between silanized and nonsilanized samples, which indicates that silanization has no influence on the thermal stability of CFs. In both silanized fiber samples, the last T_{peak} values attributed to the lignin degradation were slightly lower (minor Δ_{m_3} values) than in the corresponding nonsilanized samples, according to the lining removal during the acetone washing step of the silanization process previously described. Finally, it can be observed that the final mass residue in the silanized fibers was significantly ($p < 0.05$) higher than in the nonsilanized ones, which could be related to the amount of Si anchored on the cellulose chains.

3.2. Melt-Mixing of PBS/CF Composites

Figure 3 shows the torque versus time curves of the different PBS formulations with CFs during the melt-mixing process carried out, in all cases, at 150 °C and 50 rpm for 5 min. This residence time was selected to process all formulations in order to achieve sufficient fiber mixing in the composites but also avoid thermomechanical degradation.[38] The curves showed that, during processing, the torque sharply increased from the moment the material was fed in the mixing chamber until the biopolymer pellets plasticized and melted. Once melted, the torque progressively decreased and then reached a plateau, whose final value is associated to the melt viscosity at the selected processing conditions. Although all the formulations presented similar curves, the CF-containing samples showed higher values of plateau torque than the neat PBS sample due to fiber interactions in the melt. After 2 min of processing, the torque values in the neat PBS sample were slightly lower (≈4 N m) than in the composites (≈5 N m). All composite formulations exhibited similar values regardless the extraction method followed to obtain the fibers or the silanization process. Thus, the silanized fibers exhibited similar flow interactions with the molten biopolymer than the nonsilanized ones.

3.3. Microstructure of PBS/CF Composites

Figure 4 shows optical microscopy images taken at 40x of the PBS composite films prepared by thermo-compression. One can observe that CFs were dispersed within the PBS matrix in the form of fiber bundles with different sizes and degrees dispersion. In the film samples containing the nonfunctionalized fibers (Figure 4a,b), a higher amount of fiber agglomerates can be appreciated. Interestingly, the composite film samples with the silanized fibers (Figure 4c,d) exhibited fiber bundles with lower sizes and better dispersed in the biopolyester. The better dispersion attained for the silanized fibers can be attributed to their

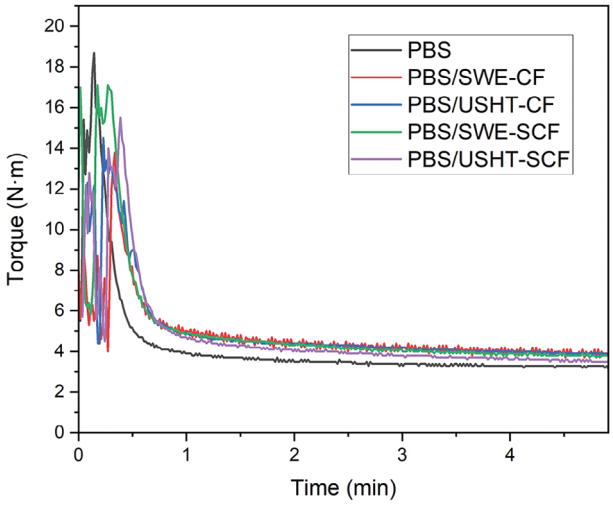

Figure 3. Development of torque (N m) as a function of time (min) during the melt-mixing of poly(butylene succinate) (PBS) with cellulose fibers obtained by subcritical water extraction and combined ultrasound-heating treatment before (SWE-CF, USHT-CF) and after silanization (SWE-SCF, USHT-SCF).

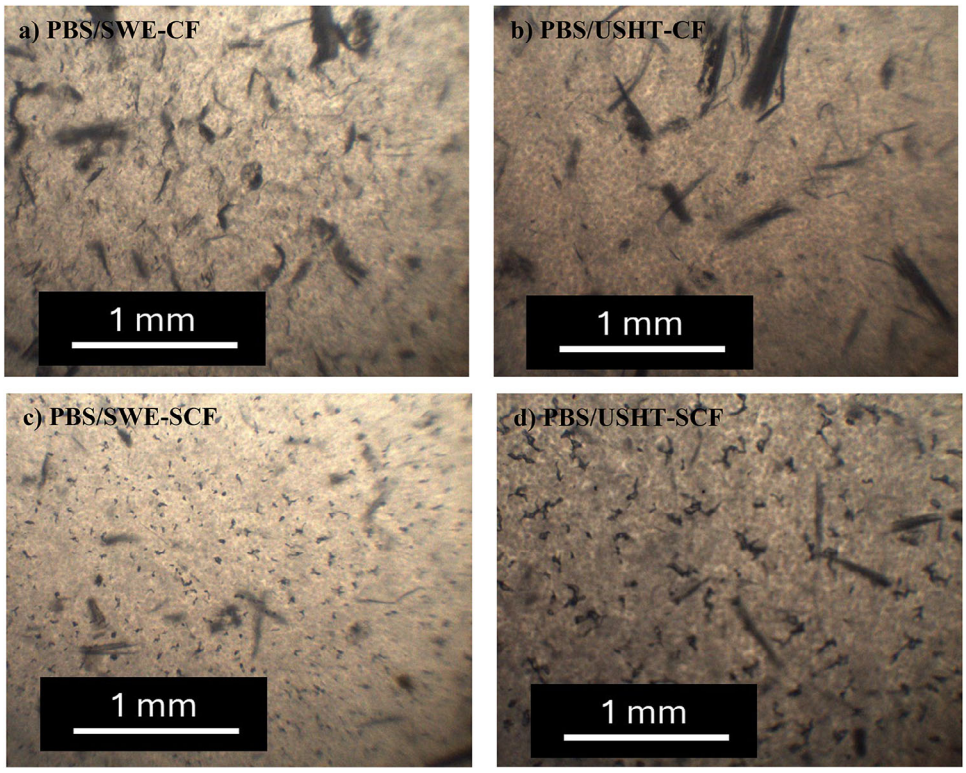

Figure 4. Optical images of the green composite films of poly(butylene succinate) (PBS) with cellulose fibers obtained by subcritical water extraction and combined ultrasound-heating treatment before and after silanization: a) PBS/SWE-CF. b) PBS/USHT-CF. c) PBS/SWE-SCF. d) PBS/USHT-SCF. Images taken at 40x with scale markers of 1 mm.

improved chemical affinity and lower interfacial adhesion with PBS.

In **Figure 5** the cross-sectional fractures attained in cryogenic conditions of PBS and its green composite films are gathered. The unfilled PBS film (Figure 5a) exhibited a smooth surface, indicating a brittle fracture, very similar to that reported by other authors.[39] At the micrograph taken at higher magnification (Figure 5b), rounded formations with rough edges were also observed, with a morphology similar to that reported for crystalline spherulites formed within the amorphous phase.[40] These structures, associated to large spherulites crystallized from the melt during cooling, are known to exhibit a morphology greatly dependent upon the crystallization temperature.[40] Observation of the surface fractures of the green composite films (Figure 5c–j) further supports that the fibers were successfully embedded in the biopolymer matrix. However, for the nonsilanized fibers (Figure 5c–f), the fiber-matrix adhesion seemed to be low, as deduced from the separation space or gap between the fibers and the biopolymer matrix (see arrows in Figure 5d,f). These morphologies were very similar to those previously reported.[25,27] In contrast, stronger interfacial adhesion forces could be deduced for the silanized fibers, where lower gaps were observed in the matrix (Figure 5g–j), according to the enhanced compatibility of the fiber by silanization. This agrees with the morphologies observed by optical microscopy and further confirms the higher miscibility attained in the green composites after fiber silanization, which favored both fiber disaggregation from the bundles and interaction with the biopolymer matrix.

3.4. Thermal and Crystallization Behavior of PBS/CF Composites

Processing conditions, fiber incorporation, and fiber silanization are all parameters that can affect the thermal behavior of PBS, which in turn highly influence on the material properties. DSC cooling and heating thermograms were obtained for all the samples to analyze the phase transitions in the biopolymer crystallization and melting temperatures as well as crystallization. Both heating and cooling thermograms are shown in **Figure 6**, which also includes the enthalpy values corresponding to the different endothermic and exothermic events.

During the first heating step (Figure 6a), one can observe that the PBS sample presented a second-order thermal transition with change in the specific heat (ΔC_p) at around 40 °C. This suggests the presence of a glass transition temperature (T_g) for PBS above room temperature that, to the best of our knowledge, has never been reported. Indeed, according to the relevant literature,[41] the main T_g for PBS is located at −44.6 °C, which will be further analyzed later by DMTA. Due to the relative high crystallinity of PBS, this second T_g can be attributed to enthalpy relaxation changes occurring at higher temperatures that result from the nonequilibrium characteristics of glass-forming molecules of the amorphous phase near the crystal lamellae. Although T_g is only associated with the amorphous phase, crystals are known to highly disturb it and then reduce the segmental mobility of the chains.[42] Thus, in semicrystalline polymers, the amorphous regions adjacent to the crystal surface can experience a higher degree of restriction. A similar interpretation of the crystal/amorphous

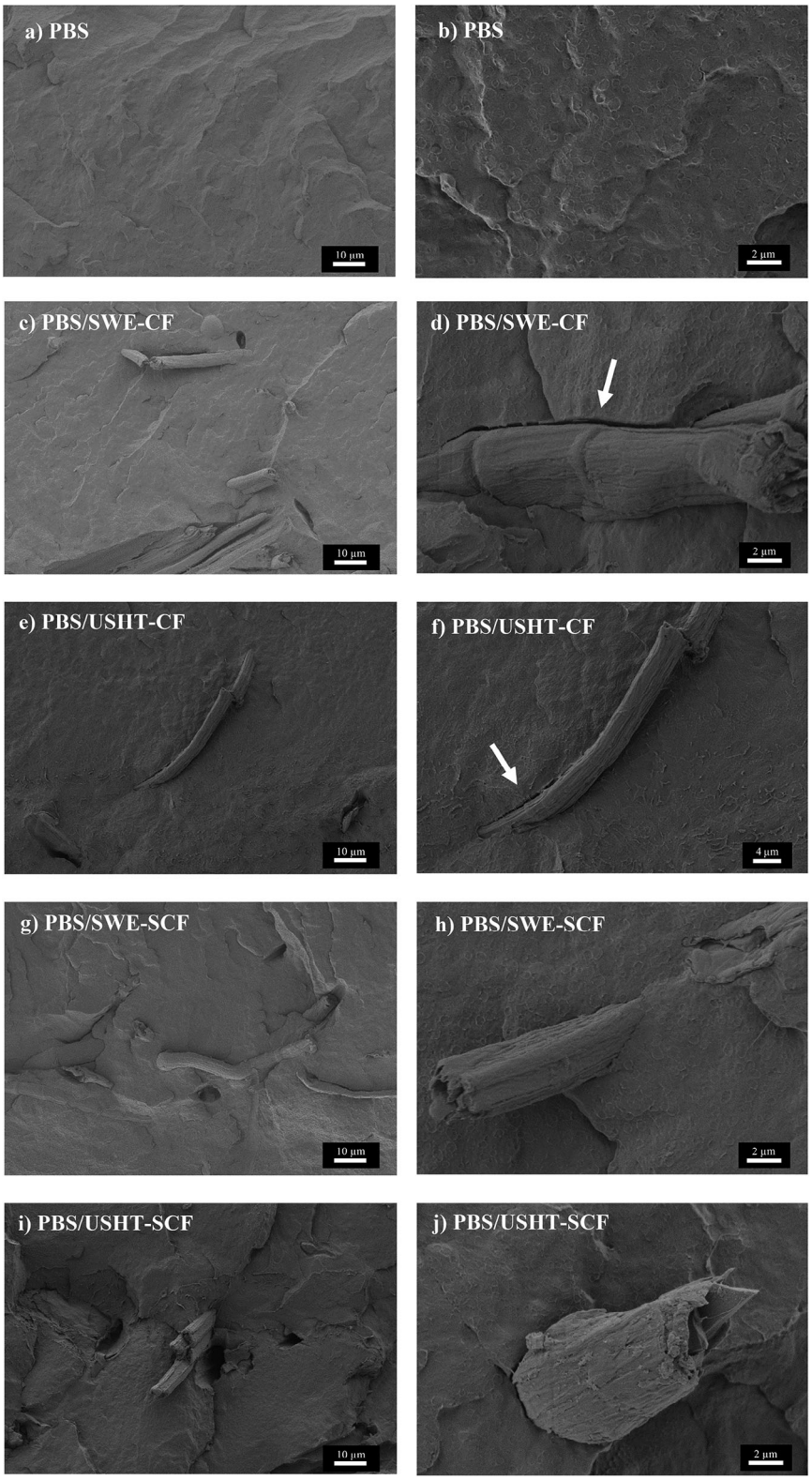

Figure 5. Field emission scanning electron microscope (FESEM) micrographs of poly(butylene succinate) (PBS) and its green composite films with cellulose fibers obtained by subcritical water extraction and combined ultrasound-heating treatment before and after silanization: a,b) PBS. c,d) PBS/SWE-CF. e,f) PBS/USHT-CF. g,h) PBS/SWE-SCF. i,j) PBS/USHT-SCF. Left images taken at 1000x and right images at 5000x with scale markers of 10 and 2 µm, respectively.

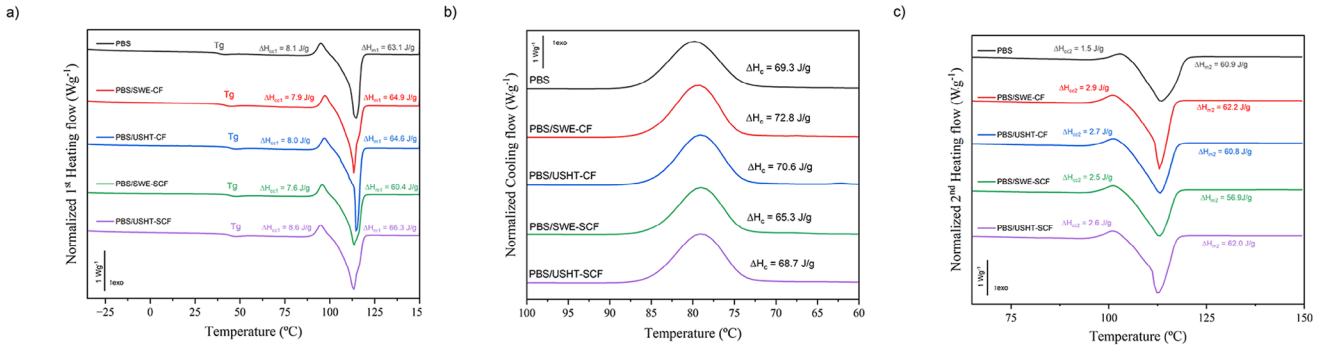

Figure 6. Differential scanning calorimetry (DSC) thermograms taken during the a) first heating. b) cooling, and c) second heating of poly(butylene succinate) (PBS) and its green composite films with cellulose fibers obtained by subcritical water extraction and combined ultrasound-heating treatment before (SWE-CF, USHT-CF) and after silanization (SWE-SCF, USHT-SCF). Enthalpy values expressed in J g^{-1} of film.

interface led to the development of a three-phase model consisting of the 1) crystalline phase, 2) a rigid amorphous fraction (RAF), and 3) a mobile amorphous fraction (MAF).[42,43] In RAF, polymer molecules remain highly entangled and partially entwined with crystalline regions. Therefore, it is suggested herein that the main glass transition region, occurring at lower temperatures, corresponds to the movement of the MAF in PBS, whereas this second one observed by DSC can be related to the molecules constituting RAF, having more segmental constraints due to their connection to the crystal surface. Furthermore, one can further observe that the T_g values shifted from 39.4 °C, in the neat PBS sample, to values in the 42–44 °C range in the CF-containing PBS samples, while slightly higher values were observed in green composites with silanized fibers (**Table 3**). This effect suggests that the fiber presence, and more notably in the case of the silanized fibers, restricted the movement of the PBS chains, which further confirms good interaction of the fibers with the biopolymer matrix. In this regard, previous studies have reported an increase in the T_g values of the amorphous phase after CF incorporation.[19]

The cooling thermograms, included in Figure 6b, indicated that PBS presents a single exothermic peak with a crystallization temperature (T_c) of 79.9 °C, which is very similar to that previously reported.[44] Fiber incorporation slightly, but still significantly ($p < 0.05$), reduced the T_c values. Lower T_c values suggest that the fibers impaired crystal formation, acting as a heterogenous antinucleating agent and this effect has been previously observed in PBS.[5] As can be seen in the first and second heating thermograms (Figure 6a,c), PBS presented a broad endothermic peak centered at 110–115 °C, corresponding to the biopolymer's melting temperature (T_m).[45] Even though the PBS samples showed a single melting peak, it took place in a broad thermal range and the peak was accompanied by a shoulder. This melting profile suggests a wide distribution of crystal sizes and varying degrees of perfection, which indicates that PBS can develop a phenomenon of double melting. The latter has been described as the effect of a continuous melting of the least perfect small crystals and their recrystallisation process with the subsequent melting at higher temperature.[46] Likewise, a small exotherm just before melting was observed in the thermograms. This peak is associated to the biopolymer's cold crystallization temperature (T_{cc}), which was seen in the range of 100–102 °C. Both the occurrence of cold crystallization and the broad melting profile evidenced that PBS presents a hindered crystallization. The incorporation of CF did not alter these characteristics since the values of T_{cc} and T_m remained nearly constant without significant differences ($p > 0.05$) among the samples (Table 3). However, the fiber presence slightly reduced the polymer crystallinity (see χ_c values in Table 3). It is then postulated that the fiber presence could not affect the crystal size and perfection, but it contributed to reduce the crystalline fraction of PBS. This fact, together with the lower T_C values, confirms the antinucleating effect of CF on PBS.

Table 3. Glass transition temperature (T_g), cold crystallization temperatures (T_{cc}), crystallization temperature (T_c), melting temperature (T_m), and crystallinity percentage (χ_c) of poly(butylene succinate) (PBS) and its green composite films with cellulose fibers obtained by subcritical water extraction and combined ultrasound-heating treatment before (SWE-CF, USHT-CF) and after silanization (SWE-SCF, USHT-SCF).

Sample	First Heating			Cooling	Second Heating		
	T_g [°C]	T_{cc} [°C]	T_{m1} [°C]	T_c [°C]	T_{cc} [°C]	T_m [°C]	χ_c [%]
PBS	$39.4 \pm 1.8^{a)}$	$95.5 \pm 0.5^{a)}$	$113.9 \pm 0.3^{a)}$	$79.9 \pm 0.1^{c)}$	$102.5 \pm 0.2^{a)}$	$113.4 \pm 0.1^{a)}$	$36.3 \pm 0.7^{c)}$
PBS/SWE-CF	$40.8 \pm 0.3^{ab)}$	$97.2 \pm 0.1^{b)}$	$113.4 \pm 0.1^{a)}$	$79.4 \pm 0.1^{b)}$	$101.4 \pm 0.5^{a)}$	$113.2 \pm 0.5^{a)}$	$35.4 \pm 0.2^{bc)}$
PBS/USHT-CF	$42.8 \pm 0.6^{b)}$	$96.8 \pm 0.2^{b)}$	$113.8 \pm 0.9^{a)}$	$78.9 \pm 0.1^{a)}$	$100.9 \pm 0.1^{a)}$	$112.6 \pm 0.2^{a)}$	$33.9 \pm 1.0^{ab)}$
PBS/SWE-SCF	$42.5 \pm 0.4^{b)}$	$95.6 \pm 0.1^{a)}$	$113.2 \pm 0.1^{a)}$	$79.1 \pm 0.1^{ab)}$	$100.9 \pm 0.1^{a)}$	$112.7 \pm 0.1^{a)}$	$31.9 \pm 0.2^{a)}$
PBS/USHT-SCF	$43.5 \pm 0.2^{b)}$	$95.1 \pm 0.3^{a)}$	$113.7 \pm 0.6^{a)}$	$78.9 \pm 0.1^{a)}$	$101.4 \pm 0.3^{a)}$	$113.2 \pm 0.4^{a)}$	$35.1 \pm 1.2^{bc)}$

[a–c)] Different superscripts in the same column indicate significant differences between samples ($p < 0.05$).

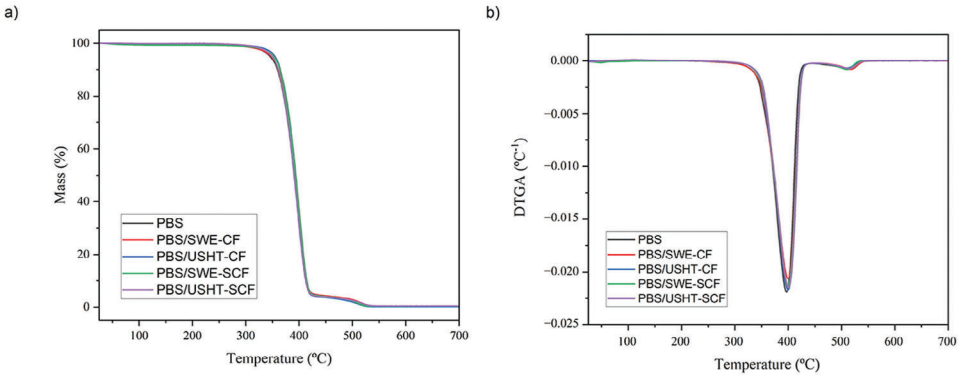

Figure 7. a) Thermogravimetric analysis (TGA) and b) first derivative thermogravimetric analysis (DTGA) curves of poly(butylene succinate) (PBS) and its green composite films with cellulose fibers obtained by subcritical water extraction and combined ultrasound-heating treatment with water reflux extraction before (SWE-CF, USHT-CF) and after silanization (SWE-SCF, USHT-SCF).

In terms of thermal stability, **Figure 7** shows TGA curves (Figure 7a) and their corresponding DTGA curves (Figure 7b) of the PBS films. **Table 4** includes the thermal stability values obtained from the TGA and DTGA curves. No significant differences ($p > 0.05$) were found among the film samples and, in all cases, thermal degradation started at ≈352 °C with a maximum degradation rate at nearly 400 °C. Furthermore, an additional mass loss in the 500–600 °C range was observed, which has been ascribed to the thermal decomposition of the organic mass produced during the previous steps.[47] Therefore, neither cellulose or the bound water contained in cellulose contributed to hydrolyze PBS. In this regard, one should consider that the biopolyester is very susceptible to hydrolysis since a water content of up to 0.1% can lead to the hydrolysis at high temperature.[48]

3.5. Mechanical Properties of PBS/CF Composites

The mechanical properties of the films were determined by tensile tests. The typical stress versus strain curves of the films are shown in **Figure 8**, whereas the tensile parameters are summarized in **Table 5**. The PBS films showed a mechanical behavior typical of rigid films with low ductility and breaking with a relatively low plastic deformation. This mechanical performance is aligned with the DSC results commented on above, which corresponds to a material with high crystallinity and regions in a glassy state at room temperature. Thus, PBS films behave as a glassy material with a high crystalline fraction. In particular, the elastic modulus (E) and tensile strength (σ_{max}) of the neat PBS films were 337.9 and 41.5 MPa, respectively, while elongation at break (ε_b) was 19.1%. These mechanical parameters were in the range of those reported by Guidotti et al.[49] (300, 16 MPa, and 5%, respectively), although the present films were slightly stiffer and resistant to break and more extensible. The incorporation of 3% wt of both SWE-CF and USHT-CF into PBS promoted the film stiffness, increasing the E value to over 480 MPa but reducing σ_{max} and ε_b to ≈30 MPa and 11%, respectively. This is the common impact of reinforcing rigid fillers incorporated into a softer polymer matrix. The silanized fibers better promoted the film elastic modulus and also better preserved the film ductility characteristics. In particular, the best mechanical performance was achieved in the PBS/SWE-CF film, which showed values of

Table 4. Thermal decomposition events detected for poly(butylene succinate) (PBS) and its green composite films with cellulose fibers obtained by subcritical water extraction and combined ultrasound-heating treatment before (SWE-CF, USHT-CF) and after silanization (SWE-SCF, USHT-SCF).

Sample	[350–450] °C			[450–700] °C	
	T_{onset} [°C]	T_{peak} [°C]	T_{final} [°C]	T_{peak} [°C]	Residue [%]
PBS	351.9 ± 4.0[a)]	396.9 ± 0.1[a)]	420.7 ± 1.8[a)]	524.6 ± 6.1[b)]	0.24 ± 0.18[a)]
PBS/SWE-CF	350.9 ± 3.8[a)]	397.5 ± 3.1[a)]	421.0 ± 2.5[a)]	516.0 ± 1.2[ab)]	0.58 ± 0.15[a)]
PBS/USHT-CF	352.5 ± 2.9[a)]	398.1 ± 2.2[a)]	420.9 ± 1.1[a)]	506.6 ± 6.7[a)]	0.31 ± 0.18[a)]
PBS/SWE-SCF	353.0 ± 3.1[a)]	398.5 ± 1.7[a)]	421.9 ± 1.9[a)]	509.5 ± 2.6[a)]	0.49 ± 0.06[a)]
PBS/USHT-SCF	352.2 ± 2.6[a)]	398.8 ± 2.1[a)]	423.0 ± 1.8[a)]	516.6 ± 2.7[ab)]	0.66 ± 0.36[a)]

[a–b)] Different superscripts in the same column indicate significant differences between samples ($p < 0.05$).

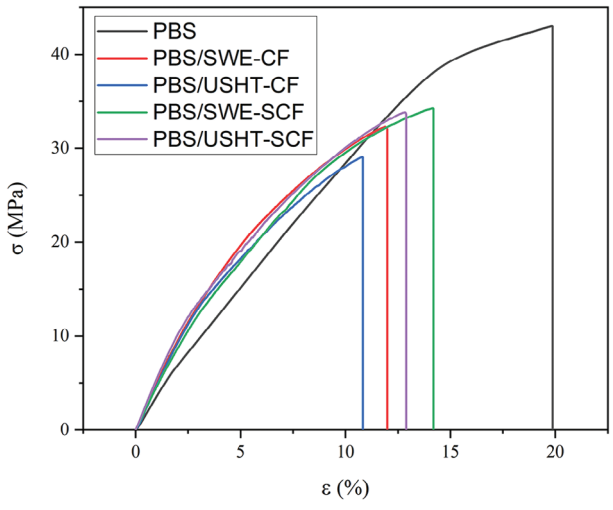

Figure 8. Tensile strength (σ) versus strain (ε) curves of poly(butylene succinate) (PBS) and its green composite films with cellulose fibers obtained by subcritical water extraction and combined ultrasound-heating treatment before (SWE-CF, USHT-CF) and after silanization (SWE-SCF, USHT-SCF).

Table 5. Elastic modulus (E), maximum tensile strength (σ_{max}), and elongation at break (ε_b) of poly(butylene succinate) (PBS) and its green composite films with cellulose fibers obtained by subcritical water extraction and combined ultrasound-heating treatment before (SWE-CF, USHT-CF) and after silanization (SWE-SCF, USHT-SCF).

Sample	E [MPa]	σ_{max} [MPa]	ε_b [%]
PBS	337.9 ± 55.5[a)]	41.5 ± 1.6[a)]	19.1 ± 1.5[c)]
PBS/SWE-CF	480.9 ± 33.2[b)]	31.6 ± 1.3[c)]	11.9 ± 0.6[a)]
PBS/USHT-CF	481.8 ± 29.6[b)]	29.3 ± 0.3[d)]	10.9 ± 0.3[a)]
PBS/SWE-SCF	474.8 ± 30.4[b)]	33.6 ± 1.9[b)]	14.1 ± 2.0[b)]
PBS/USHT-SCF	486.6 ± 39.0[b)]	30.8 ± 1.9[cd)]	12.2 ± 1.2[a)]

[a–d)] Different superscripts in the same column indicate significant differences between samples ($p < 0.05$).

474.8, 33.6 MPa, and 14.1% for E, σ_{max}, and ε_b, respectively. This represents an increase of 44% in elasticity with respect to the unfilled PBS film and of 18% in ductility when compared with the composite film with nonsilanized fibers. This improvement can be related to the better adhesion or interaction between the PBS matrix and the anchored GPS-cellulose, as described previously during the morphological analysis of the composite films. Liminana et al.[50] achieved comparable results using two reactive compatibilizers, namely epoxidized linseed oil (ELO) and epoxidized soybean oil (ESBO), in PBS sheets reinforced with almond shell flour (ASF).

3.6. Thermomechanical Properties of PBS/CF Composites

DMTA assays were carried out in the film samples from −50 to 100 °C in order to better elucidate the effect of fiber incorporation on the mechanical response as well as to better ascertain the glass transition region of PBS. The storage modulus (E'), loss modulus (E''), and damping factor ($tan\ \delta$) were obtained by submitting the material to dynamic loading involving periodic oscillations while increasing temperature. **Figure 9** shows the evolution of these three parameters as a function of temperature. The changes in E' are associated to the elastic response of the films, which can be observed as function of temperature in Figure 9a. At −50 °C, the neat PBS film showed a value of E' of ≈3 GPa, whereas the composite films exhibited higher values (in the 3.5–3.8 GPa range). This confirms the mechanical reinforcing effect produced by the fibers on PBS. As the temperature increased to 0 °C, an expected decrease in the E' values was observed in all the film samples due to a softening effect of the PBS matrix. The latter is associated to the main segmental relaxation or (α)-relaxation of the polyester (glass transition). After glass transition, the unfilled PBS film reached an E' value of ≈350 MPa at 0 °C, whereas the composite films exhibited higher values, near 650 MPa. Thereafter, the E' values of the neat PBS film reduced progressively, the values of the green composite films being always higher. In this thermal range, the SWE-CF-containing PBS films slightly outperformed the composites with USHT-CF, while the highest performance was attained for the PBS/SWE-SCF film. This finding agrees with the better interfacial adhesion attained between the silanized fibers and the biopolymer matrix, which was also consistent with the mechanical performance obtained from the tensile tests. A slight increase in E' was observed at temperatures close to 90 °C, which can be ascribed to the cold crystallization phenomenon commented during the DSC analysis. Finally, from 100 °C, the E' values sharply decreased due to partial melting of the less perfect PBS crystals. Similar DMTA patterns were reported for PBS by other authors.[51]

The development of loss modulus (E'') as a function of temperature (Figure 9b) reflected that all the film samples exhibited a sharp peak during the α-transition related to the biopolymer's T_g. This thermomechanical change is proportional to the energy dissipated in the films during the loading cycle and confirms that the main glass–rubber transition of PBS takes place at ≈−30 °C in all samples, regardless the fiber presence. Analogous observations were found for the $tan\ \delta$ values, shown in Figure 9c, which represents the ratio of the energy lost to the energy stored in the cyclic deformation. In particular, a broad and intense relaxation was observed for the neat PBS film, centered at around −25.4 °C, which is very similar to that reported in the study of Liminana et al.,[50] where the $tan\ \delta$ peak was located between −21 and −31 °C. Therefore, PBS undergoes a glass transition below room temperature. However, one can observe an additional low-intense relaxation peak centered at nearly 51 °C, which confirms the existence of a secondary relaxation process that takes places in certain rubber-like regions of PBS, as previously described during the DSC analysis. As concerns the green composite films, similar $tan\ \delta$ peaks were observed, but with lower intensity and slightly delayed to higher temperatures. This difference in the thermomechanical behavior implies that the CF-containing samples presented lower

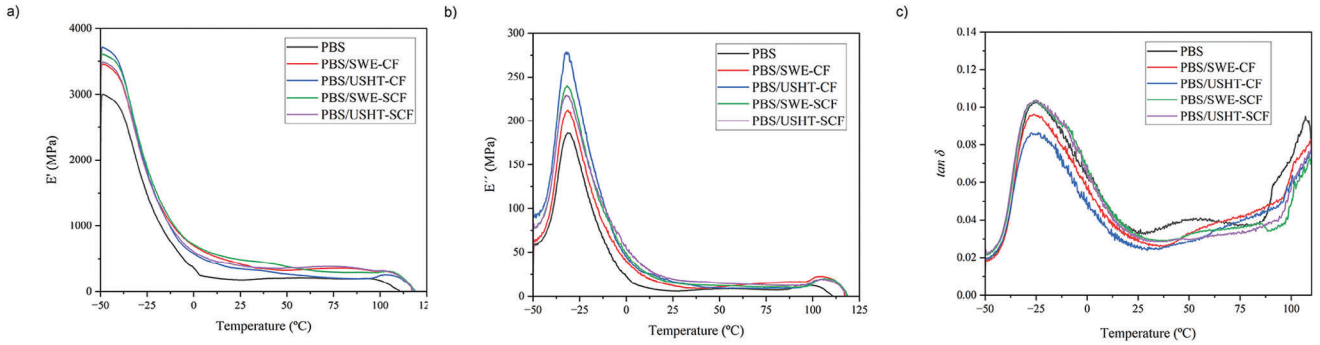

Figure 9. a) Storage modulus (E'), b) loss modulus (E''), and c) damping factor ($tan\ \delta$) of poly(butylene succinate) (PBS) and its green composite films with cellulose fibers obtained by subcritical water extraction and combined ultrasound-heating treatment before (SWE-CF, USHT-CF) and after silanization (SWE-SCF, USHT-SCF).

Table 6. Permeability to water vapor (WVP) and oxygen (OP) of poly(butylene succinate) (PBS) and its green composite films with cellulose fibers obtained by subcritical water extraction and combined ultrasound-heating treatment before (SWE-CF, USHT-CF) and after silanization (SWE-SCF, USHT-SCF).

Sample	WVP x 10^{14} [kg m^{-1} Pa s m^2]	OP x 10^{18} [m^3 m m^{-2} s Pa]
PBS	$1.88 \pm 0.07^{a)}$	$1.08 \pm 0.05^{b)}$
PBS/SWE-CF	$2.04 \pm 0.05^{ab)}$	$0.89 \pm 0.03^{a)}$
PBS/SWE-SCF	$2.25 \pm 0.03^{bc)}$	$0.87 \pm 0.03^{a)}$
PBS/USHT-CF	$2.55 \pm 0.07^{b)}$	$1.24 \pm 0.08^{c)}$
PBS/USHT-SCF	$2.96 \pm 0.19^{c)}$	$0.93 \pm 0.08^{ab)}$

[a–c)] Different superscripts in the same column indicate significant differences between samples ($p < 0.05$).

energy dissipation and potentially lower toughness due to the biopolymer chain movement restriction by the presence of fibers.

3.7. Barrier and Hydrophobic Properties of PBS/CF Composites

The values of WVP and OP of the PBS films are shown in **Table 6**. The barrier performance to water vapor and oxygen is, in fact, of main interest for food packaging. Whereas water vapor barrier is of great importance to avoid food physical and chemical deteriorations related to changes in the moisture content, oxygen barrier properties are particularly relevant in foodstuffs sensible to oxidation processes (e.g., meat, fish, or high-lipid-content products). In this regard, succinic acid derived biopolyesters are known to show medium barrier to water vapor but medium-to-low barrier to oxygen.[4]

The neat PBS film exhibited a WVP value of 1.88×10^{-14} kg m m^{-2} Pa s at 25 °C and 53% RH. This value is in the range of that reported by other authors, for instance, 4.93×10^{-14} kg m m^{-2} Pa s (25 °C, 53% RH)[39] and 1.53×10^{-14} kg m m^{-2} Pa s (25 °C, 53% RH)[51] and slightly lower than that recently attained for PBS blends with poly(butylene succinate-*co*-adipate) (PBSA), that is, 3.15×10^{-14} kg m m^{-2} Pa s (25 °C, 53% RH).[4] This permeability value is approximately six times higher than that of the commercial polyester polyethylene terephthalate (PET), that is, 3.01×10^{-15} kg m m^{-2} Pa s (at 0% RH and 25 °C)[52] and one order of magnitude higher than that of water-vapor-high-barrier polyolefins, such as low-density polyethylene (LDPE) (1.20×10^{-15} kg m m^{-2} Pa s) and polypropylene (PP) (0.73×10^{-15} kg m m^{-2} Pa s) (38 °C, 90% RH).[53] Compared to the main biodegradable polyesters, the water vapor barrier properties of PBS is lower than that of poly(3-hydroxybutyrate-*co*-3-hydroxyvalerate) (PHBV) (1.82×10^{-15} kg m m^{-2} Pa s) and in between of that of PLA (1.23×10^{-14} kg m m^{-2} Pa s) and poly(butylene adipate-*co*-terephthalate) (PBAT) (3.31×10^{-14} kg m m^{-2} Pa s) (25 °C, 0% RH).[54] Fiber incorporation slightly but significantly ($p < 0.05$) reduced the water-vapor barrier of PBS because cellulose is a hydrophilic material with large number of free —OH groups. Furthermore, silanization did not improve the water–vapor barrier of the CF-containing films, but slightly increased the values. This result can be due to the fact that fibers were more exposed to water circulating the PBS matrix due to these were better dispersed, as previously demonstrated during the morphological analysis. The highest permeability, that is, lowest barrier, was attained for the USHT-CF-containing PBS films, reaching values close to 3 $\times 10^{-14}$ kg m m^{-2} Pa s. This poor performance can be related to their higher hemicellulose content that exhibits more hygroscopic character in line with its amorphous nature.

The changes in the hydrophobicity of the PBS films by the fiber incorporation was confirmed by the analysis of the water-contact angle. **Figure 10** illustrates the water drops deposited on the surface of the PBS and its green composite films. It also includes the values of the water contact angles, where the higher the angle the more hydrophobic the material. For the neat PBS film, contact angle was nearly 63°, which corresponds to a relatively hydrophobic material surface. This value is similar to that reported by Totaro et al.[55] (62.5°) and lower than that obtained by Yan et al.[56] (76.81°). The contact angle was significantly ($p < 0.05$) reduced when the USHT fibers were incorporated into the biopolymer, whereas no significant differences ($p > 0.05$) were produced for the SWE fibers. As indicated above, this must be mainly attributed to the higher hemicellulose content of USHT fibers and its greater hydrophilic nature.

In terms of oxygen barrier, the neat PBS exhibited an OP value of 1.08×10^{-18} m^3 m m^{-2} Pa s at 25 °C and 53% RH. This value is similar but slightly lower than that found previously for PBS, that is, 1.78×10^{-18} m^3 m m^{-2} Pa s (25 °C, 50% RH)[51] and, as expected, than that reported for PBS/PBSA blends, that is, 1.27×10^{-18} m^3 m m^{-2} Pa s (25 °C, 53% RH).[4] Fiber incorporation significantly ($p < 0.05$) increased the oxygen-barrier performance of PBS. This positive effect was most noticeable in the case of the PBS films filled with SWE fibers, either with or without silanization treatment. In particular, the highest oxygen barrier enhancement was obtained for the PBS/SWE-SCF film, with an OP value of 0.87×10^{-18} m^3 m m^{-2} Pa s, which represents a percentage increase of nearly 20% in the performance versus the unfilled PBS film. This barrier improvement derives from the effective dispersion of CFs within the PBS matrix, which provides a

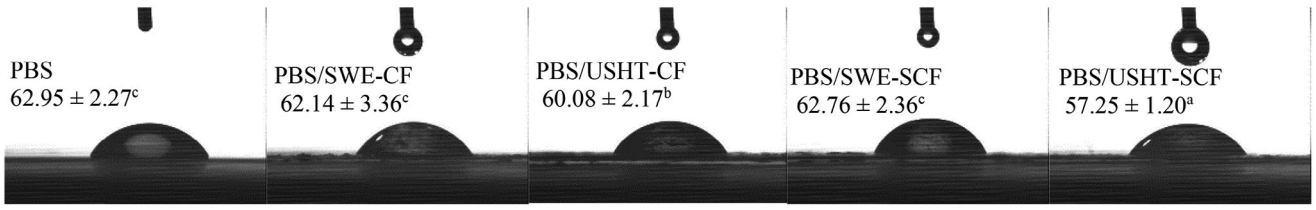

[a–c] Different superscripts indicate significant differences between samples ($p < 0.05$)

Figure 10. Water contact images and angles of poly(butylene succinate) (PBS) and its green composite films with cellulose fibers obtained by subcritical water extraction and combined ultrasound-heating treatment before (SWE-CF, USHT-CF) and after silanization (SWE-SCF, USHT-SCF).

tortuous path for the diffusion of oxygen molecules and consequently leads to a decrease in permeability. The resultant barrier properties against oxygen puts these green composite films in the range of medium-oxygen-barrier materials, only one range lower than that of PHBV (2.1×10^{-19} m^3 m m^{-2} Pa s) measured at 25 °C and 60% RH[54] and PET films measured at 23 °C and 0% RH (3.27×10^{-19} m^3 m m^{-2} Pa s) and 75% RH (4.26×10^{-19} m^3 m m^{-2}· Pa s).[52] These films are two to three orders of magnitude more permeable than oxygen-barrier polymers such as polyamide 6 (PA6) ($0.52–2.5 \times 10^{-19}$ m^3 m m^{-2} Pa s measured at 23 °C and 0–75% HR) and poly(ethylene-*co*-vinyl alcohol) (EVOH) ($0.77–91 \times 10^{-21}$ m^3 m m^{-2}· Pa s measured at 23 °C and 0–75% HR), but are less affected by humidity due its higher water–vapor barrier. Moreover, the green composite films successfully outperform the barrier performance against oxygen of most biopolymers, such as PLA (2.22×10^{-18} m^3 m m^{-2} Pa s) and PBAT (9.14×10^{-17} m^3 m m^{-2}· Pa s) measured at 25 °C and 60% RH.[54]

4. Conclusions

In this study, SWE and USHT were both demonstrated as effective green solvent extraction techniques for obtaining CFs. Among the two methods, SWE was more effective to selectively remove hemicelluloses, while the lignin content was similar in both bleached fibers. Both fibers were thereafter silanized using GPS and then incorporated at 3% wt into PBS by melt-mixing. Silanization both promoted the removal of lignin and successfully contributed to better increase the compatibility of the fibers with PBS. The high dispersion and interaction between the fibers and the biopolyester successfully resulted in materials with enhanced rigidity and oxygen barrier performance. It was noticed that the fiber presence reduced the mobility of the PBS chains in the amorphous regions. In this regard, it was originally revealed the presence of a second glass transition region for PBS located above room temperature, which was ascribed to movement of the biopolyester molecules constituting RAF, having more segmental constraints due to their connection to the crystal surface. These molecules with restricted movement are considered to contribute to the low ductility of the biopolyester observed at room temperature.

Therefore, the valorization of rice straw wastes by green extraction methods are very promising for developing CFs that can be latter silanized and applied to reinforce biodegradable materials. In the case of PBS, the resultant materials can be of interest for rigid food packaging, in applications where high rigidity and moderate barrier to water vapor and oxygen are required. Future studies will deal with the optimization of the fiber content and the evaluation of the thermo-compressed composite films in packaging applications to preserve foodstuffs.

Acknowledgements

This research was funded by the Spanish Ministry of Science and Innovation (MICI), Grant No. PID2021-128749OB-C33, and Generalitat Valenciana (GVA), Grant Nos. AGROALNEXT/2022/026 and CIPROM/2021/071. Sergio Torres-Giner also acknowledged the financial support received during his Ramón y Cajal contract (RYC2019-027784-I) and Carmen Olivas-Alonso during her PhD scholarship (No. CIACIF/2021/422).

Conflict of Interest

The authors declare no conflict of interest.

Data Availability Statement

The data that support the findings of this study are available from the corresponding author upon reasonable request.

Keywords

green composites, green extraction methods, renewable succinic acid derived polyesters, sustainable materials, waste valorization

Received: March 12, 2024
Revised: June 20, 2024
Published online:

[1] S. Torres-Giner, *Appl. Sci.* **2023**, *13*, 5864.
[2] D. Verma, V. Dogra, A. K. Chaudhary, R. Mordia, *Sustainable Biopolymer Composites: Biocompatibility, Self-Healing, Modeling, Repair and Recyclability: A Volume in Woodhead Publishing Series in Composites Science and Engineering*, Elsevier, Amsterdam **2022**, pp. 113–128.
[3] S. Bello, D. Ladakis, S. González-García, G. Feijoo, A. Koutinas, M. T. Moreira, *Chem. Eng. J.* **2022**, *428*, 132011.
[4] E. Hernández-García, M. Pacheco-Romeralo, P. Zomeño, G. Viscusi, F. Malvano, G. Gorrasi, S. Torres-Giner, *Materials* **2023**, *16*, 3872.
[5] A. Gowman, T. Wang, A. Rodriguez-Uribe, A. K. Mohanty, M. Misra, *ACS Omega* **2018**, *3*, 15205.
[6] S. Kangishwar, N. Radhika, A. A. Sheik, A. Chavali, S. A. Hariharan, *Polym. Bull.* **2023**, *80*, 47.
[7] P. A. V. Freitas, C. González-Martínez, A. Chiralt, *Innovative Food Sci. Emerging Technol.* **2022**, *76*, 102932.
[8] Y. D. Li, Q. Q. Fu, M. Wang, J. B. M. Zeng, *Carbohydr. Polym.* **2017**, *164*, 75.
[9] P. A. V. Freitas, C. González-Martínez, A. Chiralt, *Carbohydr. Polym.* **2023**, *312*, 120805.
[10] E. S. Ong, J. S. H. Cheong, D. Goh, *J. Chromatogr. A* **2006**, *1112*, 92.
[11] M. Plaza, M. Amigo-Benavent, M. D. del Castillo, E. Ibáñez, M. Herrero, *Food Res.* **2010**, *43*, 2341.
[12] Z. Tang, Y. Wang, G. Huang, H. Huang, *Ultrason. Sonochem.* **2023**, *97*, 106474.
[13] M. Stepanova, E. Korzhikova-Vlakh, *Polymers* **2022**, *14*, 1477.
[14] E. Vatansever, D. Arslan, M. Nofar, *Int. J. Biol. Macromol.* **2019**, *137*, 912.
[15] T. Bin, J. P. Qu, L. M. Liu, Y. H. Feng, S. X. Hu, X. C. Yin, *Thermochim. Acta* **2011**, *525*, 141.
[16] Z. Wang, X. Qiao, K. Sun, *Carbohydr. Polym.* **2018**, *197*, 442.
[17] J. Liu, X. Xie, L. Li, *Constr. Build Mater.* **2022**, *347*, 128575.
[18] M. J. Mochane, S. I. Magagula, J. S. Sefadi, T. C. Mokhena, *Polymers* **2021**, *13*, 1200.
[19] F. Liu, S. Lu, W. Cao, J. Huang, Y. Sun, Y. Xu, M. Chen, H. Na, J. Zhu, *Polymers* **2022**, *14*, 3449.
[20] S. Dev S. Kopparthy, *M.Sc. Thesis*., Cornell University, New York **2021**.
[21] A. M. Noor Azammi, R. A. Ilyas, S. M. Sapuan, R. Ibrahim, M. S. N. Atikah, M. Asrofi, A. Atiqah, *Interfaces in Particle and Fibre Reinforced Composites: Current Perspectives on Polymer, Ceramic, Metal and Extracellular Matrices*, Elsevier, Amsterdam **2019**, pp. 29–93.

[22] Á. Agüero, D. Garcia-Sanoguera, D. Lascano, S. Rojas-Lema, J. Ivorra-Martinez, O. Fenollar, S. Torres-Giner, *Polymers* **2020**, *12*, 821.
[23] Y. Xie, C. A. S. Hill, Z. Xiao, H. Militz, C. Mai, *Composites, Part A* **2010**, *41*, 806.
[24] I. C. Cabrera, S. Berlioz, A. Fahs, G. Louarn, P. Carriere, *Int. J. Biol. Macromol.* **2020**, *165*, 1773.
[25] L. Liu, J. Yu, L. Cheng, X. Yang, *Polym. Degrad. Stab.* **2009**, *94*, 90.
[26] A. Valadez-Gonzalez, J. M. Cervantes-Uc, R. Olayo, P. J. Herrera-Franco, *Composites, Part B* **1999**, *30*, 309.
[27] Y. Zhao, J. Qiu, H. Feng, M. Zhang, *J. Appl. Polym. Sci.* **2012**, *125*, 3211.
[28] B. P. Calabia, F. Ninomiya, H. Yagi, A. Oishi, K. Taguchi, M. Kunioka, M. Funabashi, *Polymers* **2013**, *5*, 128.
[29] A. Sluiter, B. Hames, R. Ruiz, C. Scarlata, J. Sluiter, D. Templeton, D. Crocker, Determination of Structural Carbohydrates and Lignin in Biomass: Laboratory Analytical Procedure (LAP), Issue Date: 7/17/2005, **2008**.
[30] T. Ferreira, W. Rasband, Image J user Guide 2012, 676, 1.46r.
[31] P. A. V. Freitas, C. I. La Fuente Arias, S. Torres-Giner, C. González-Martínez, A. Chiralt, *Appl. Sci.* **2021**, *11*, 8433.
[32] K. Chen, P. Li, X. Li, C. Liao, X. Li, Y. Zuo, *Int. J. Biol. Macromol.* **2021**, *182*, 2108.
[33] American Society for Testing and Materials, ASTMD E96/E96M –16, Standard Test Methods for Water Vapor Transmission of Materials, **2021**, *1*.
[34] Q. Wu, F. Yao, X. Xu, C. Mei, D. Zhou, *J. Ind. Eng. Chem.* **2013**, *19*, 670.
[35] H. Yang, R. Yan, H. Chen, D. H. Lee, C. Zheng, *Fuel* **2007**, *86*, 1781.
[36] R. Requena, A. Jiménez-Quero, M. Vargas, R. Moriana, A. Chiralt, F. Vilaplana, *ACS Sustain. Chem. Eng.* **2019**, *7*, 6275.
[37] D. Theng, G. Arbat, M. Delgado-Aguilar, B. Ngo, L. Labonne, P. Evon, P. Mutjé, *Ind. Crops Prod.* **2017**, *107*, 184.
[38] P. A. V. Freitas, H. Barrrasa, F. Vargas, D. Rivera, M. Vargas, S. Torres-Giner, *Appl. Sci.* **2022**, *12*, 2111.
[39] A. Costa, A. Crocitti, M. Malinconico, G. Santagata, P. Cerruti, *Properties of Biodegradable Films Based on Poly(Butylene Succinate) (PBS) and Poly(Butylene Adipate-co-Terephthalate) (PBAT) Blends. In Polymers*, Vol. *1981*, American Institute of Physics Inc., College Park, MD, USA **2020**.
[40] Z. Gan, H. Abe, Y. Doi, *Biomacromolecules* **2001**, *2*, 313.
[41] H. M. Ye, R. D. Wang, J. Liu, J. Xu, B. H. Guo, *Macromolecules* **2012**, *45*, 5667.
[42] L. C. E. Struik, *Polymer* **1987**, *28*, 1521.
[43] D. Heidrich, M. Gehde, *Polymers* **2022**, *14*, 793.
[44] S. Chen, X. Peng, L. Geng, H. Wang, J. Lin, B. Chen, A. Huang, *Sci. Rep.* **2021**, *11*, 6802.
[45] P. L. D. Gregori, *Composites, Part B* **2018**, *144*, 153.
[46] Y. J. Phua, N. S. Lau, K. Sudesh, W. S. Chow, Z. A. Mohd Ishak, *Polym. Degrad. Stab.* **2012**, *97*, 1345.
[47] M. Ndiaye, P. Myler, B. K. Kandola, *J. Compos. Sci.* **2022**, *6*, 27.
[48] J. Xu, B. H. Guo, *Biotechnol. J.* **2010**, *5*, 1149.
[49] G. Guidotti, M. Soccio, V. Siracusa, M. Gazzano, E. Salatelli, A. Munari, N. Lotti, *Polymers* **2017**, *9*, 724.
[50] P. Liminana, D. Garcia-Sanoguera, L. Quiles-Carrillo, R. Balart, N. Montanes, *Composites, Part B* **2018**, *144*, 153.
[51] N. Bumbudsanpharoke, P. Wongphan, K. Promhuad, P. Leelaphiwat, N. Harnkarnsujarit, *Food Control* **2022**, *132*, 108541.
[52] E. Gabirondo, B. Melendez-Rodriguez, C. Arnal, J. M. Lagaron, A. Martínez De Ilarduya, H. Sardon, S. Torres-Giner, *Polym. Chem.* **2021**, *12*, 1571.
[53] J.-M. Lagarón, *Multifunctional and Nanoreinforced Polymers for Food Packaging*, Woodhead Publishing, Cambridge **2011**.
[54] L. Quiles-Carrillo, N. Montanes, J. M. Lagaron, R. Balart, S. Torres-Giner, *J. Polym. Environ.* **2019**, *27*, 84.
[55] G. Totaro, L. Sisti, M. Fiorini, I. Lancellotti, F. N. Andreola, A. Saccani, *J. Polym. Environ.* **2019**, *27*, 1488.
[56] Y. Yan, Q. Dou, *Starch* **2021**, *73*, 2000184.

